Paper number : 132

Application of Continuation and Bifurcation Methods to Aeroelastic Rotor Blade Stability

Djamel Rezgui
AgustaWestland/Bristol University Technology Centre
Dept. of Aerospace Engineering
University of Bristol, UK
djamel.rezgui@bris.ac.uk

Mark H. Lowenberg
Dept. of Aerospace Engineering
University of Bristol, UK
m.lowenberg@bris.ac.uk

Mark Jones
AgustaWestland Ltd, Yeovil, Somerset, UK
mark.jones@agustawestland.com

Claudio Monteggia
AgustaWestland SPA, Cascina Costa, Italy
claudio.monteggia@agustawestland.com

Abstract

The present paper illustrates how continuation and bifurcation methods are applied to investigate the aeroelastic stability of helicopter blades over a range of flight and control parameters. The paper first compares the bifurcation results for flap-lag instability to those available in the literature, which are obtained using conventional methods. In this case, the continuation analysis is applied to a simple rotor system incorporating a rigid blade with flap and lag degrees of freedom with root springs to model the stiffness of hinges. The continuation analysis is then carried out to investigate the aeroelastic stability of rotor blades, where modal representation of the blade flexibility is used. The analysis is performed in hover and forward flight, within and beyond operating flight conditions. The significance of the typical bifurcations that the blade behaviour undergoes is discussed.

NOMENCLATURE

$'$	Differentiation with azimuth angle.
$\dot{(\,)}$	Differentiation with time.
A_{lat},B_{long}	Lateral and longitudinal cyclic pitch angles.
C_T	Rotor thrust coefficient.
C_L, C_D, C_M	Elemental lift, drag and pitching moment coefficients.
C_{d_0}	Blade profile drag coefficient.
L, D	Elemental aerodynamic flapwise, lagwise force components, positive upward and forward respectively.
L_0, D_0	Elemental aerodynamic flapwise and lagwise force components computed when the blade's modes are evaluated, positive upward and backward respectively.
M	Elemental aerodynamic pitching moment about the section shear centre, positive nose up.
M_0	Elemental aerodynamic pitching moment computed when the blade's modes are evaluated, positive nose up.
Ma	Elemental Mach number.
NB	Number of blades.
Q_{q_i}	Generalised force of mode i.
R	Rotor radius.
T	Rotor oscillation period.
T_i, T_{av}	Rotor instantaneous and average thrust.
T_{req}	Required rotor thrust.
U_P, U_T	Perpendicular and tangential components of the elemental flow velocity.
Ω	Rotor speed.
Θ	Blade pitch due to twist deformation.
α	Elemental angle of attack.
α_s	Rotor shaft angle.
$\bar{R}$	Elastic coupling parameter.
$\bar{f}$	Helicopter flat plate drag area.
β	Flap angle, positive upward.
$\beta_{a_1,req}$, $\beta_{b_1,req}$	Required lateral and longitudinal flapping angles.
β_{pc}	Precone angle.
δr	Width of the blade element.
δ	Parameter vector describing the rotor and flow properties.
η	negative real part of the eigenvalue associated with the lag degree-of-freedom.

γ	Lock number.
λ	Inflow ratio.
μ	Advance ratio.
ν_0, ν_s, ν_c	Average, lateral and longitudinal induced velocity components.
ν_i	Induced velocity at position r and azimuth ψ.
$\omega_\beta, \omega_\zeta$	Non-rotating flap and lead-lag frequencies.
ω_{q_i}	Modal frequency of mode i.
ϕ	Inflow angle.
ψ	Azimuth angle.
σ	Rotor solidity.
θ_{col}	Collective pitch angle.
$\theta_{pre.twist}$	Blade local built-in twist.
ζ	Lag angle, positive forward.
c	Blade elemental chord.
p	Dimensionless rotating flapping frequency at $\theta = 0$, $p = \sqrt{1+\omega_\beta^2}$.
q_i	Generalised displacement of mode i.
r	Elemental radial position.
t	Time.
u,y	Harmonic oscillator states, $u = \sin(\Omega\ t)$ and $y = \cos(\Omega\, t)$.
w_i,v_i,t_i	Flap, lag, and torsion mode shapes of mode i.
x	State vector.
I_i	Modal mass of mode i.

INTRODUCTION

The stability of a helicopter rotor blade is a complex dynamical problem, involving aerodynamic, structural, material and geometric nonlinearities. Furthermore, the trend towards higher performance gains and lower vibration and noise levels has led to the development of more complex rotor systems, which incorporate novel designs features, utilizing for example: composite materials, active lag dampers and active trailing edge flaps. These features tend to increase the levels of nonlinearity in the rotor system, which means that a proper nonlinear analysis of the blade dynamics is required. Until this time, different mathematical techniques have been used to study the aeromechanical and aeroelastic blade stability, at different flight regimes. These techniques include time history simulation (time integration techniques) [1], parametric resonance analyses [2, 3, 4, 5], perturbation methods [6, 7] and Floquet analysis [7, 8, 9]. In fact, the helicopter blade aeromechanical and aeroelastic stability is well understood in both the academic and industrial sectors, including cases of very high tip speed ratios. Extensive reviews in the field are those by Friedmann [10, 11], Bielawa [12] and Chopra [13].

However, many of the above stability methods depend on assumptions that are questionable for newer rotor configurations, or may not provide the complete stability picture. For example, the methods can predict the local stability of the blade, but the regions of attraction in that case are not defined. In other words, the blades might be stable for small disturbances but not necessarily for large ones; and hence the outcome in the event of a large disturbance inducing instability is not indicated.

In recent years, the stability of rotors in autorotation was investigated by Rezgui *et al.* and Lowenberg *et al.* using nonlinear dynamics theory implemented numerically in the form of continuation and bifurcation methods [14, 15, 16, 17]. The studies showed that these techniques are crucial in the identification of the instability scenarios of rotors in autorotation including but not exclusive to blade sailing, high speed instability, control input-induced instability and lightly loaded rotor instability. The analysis showed the presence of different bifurcation points which establish the coexistence of stable and unstable periodic solutions over a range of parameters. The analysis was complemented by wind tunnel testing, the results of which exhibited substantial agreement with those obtained from bifurcation analysis, including an unexpected asymmetric form of stable autorotation.

In the present paper, the continuation and bifurcation methods are applied to investigate the aeroelastic stability of a helicopter blade over a range of flight and control parameters. The analysis first investigates the stability of a rigid blade model and compares the bifurcation results to those available in the literature, which are obtained using conventional methods. In this case the blades are modelled to incorporate rigid lag and flap degrees of freedom with root springs to represent the stiffness of hinges. The continuation analysis was then carried out to investigate the aeroelastic stability of rotor blades, where modal representation of the blade flexibility is used.

CONTINUATION AND BIFURCATION METHODS FOR BLADE STABILITY

The basic idea of the continuation techniques is the calculation of the steady solutions of a dynamical system as one of its parameters, called the continuation parameter, is varied across a pre-defined range. The computed solutions construct a number of equilibrium branches that could be either stable or unstable. To determine the stability, either an Eigen or Floquet analysis is carried out at each computed solution, depending on the nature of this solution. For instance, in hover the blade behaviour can be said to be in equilibrium (fixed points), hence an eigen analysis is carried out for stability. Whereas, in forward flight, the blades behave in a periodic manner

(limit cycles) due to the rotor lift asymmetry, hence Floquet theory is used to determine the stability.

Bifurcation is the qualitative change in the system behaviour as a parameter is varied. In other words, when the stability of a system is changed or lost, the system bifurcates. The points at which these stability changes happen are called bifurcation points. When the system is nonlinear, new solution branches may emerge from the bifurcation points, leading to the presence of multiple solutions for the same set of system parameters. The identification of these different solution branches helps to uncover the global dynamics of the system. Particular interest is when the blades, for example, are locally stable for small disturbances but not necessarily for large ones, and vice-versa.

Therefore, the strategy in implementing continuation and bifurcation methods is to follow one solution branch as one or more parameters are varied to locate bifurcation points. Then, follow the emerging branches to construct a more complete picture of the system dynamics (bifurcation diagram). The different types of bifurcations that can occur in equilibria or periodic orbits are not discussed in this paper. However, the reader is referred to general texs such as references [18, 19] for more background on the subject.

The continuation algorithm used in this analysis is implemented in the continuation and bifurcation software AUTO [20]. Besides many other types of equations, AUTO can perform extensive bifurcation analysis of ordinary differential equations (ODEs) of the form:

$$\dot{x}(t) = f(x(t), \delta), \quad f, x \in \Re^n \tag{1}$$

subject to initial conditions, boundary conditions, and integral constraints. Here x is the state vector and δ denotes one or more parameters. Equation (1) is written in the generic (nonlinear) state-space form, where the state-derivatives are functions of the states and some parameters. Therefore, as far as AUTO is concerned, the dynamical model must be constructed in a format which allows passing the state derivatives to AUTO and receiving states and parameters from it, regardless of the environment where the system equations are coded. This software attribute provides a stability tool which not only is independent from the model but also able to couple with a wide range of modelling platforms, which can be particularly beneficial in the helicopter industry.

DESCRIPTION OF NONLINEAR ROTOR BLADE MODELS

In this paper, the continuation and bifurcation analysis is applied to two different rotor blade models. Both are modeled in the dynamical system form of Equation (1) where the parameter vector δ can hold values for blade control angles, helicopter velocities, blade properties, etc. Furthermore, the ODEs in Equation (1) are autonomous in that the independent variable t does not appear explicitly in the equations. However, in cases where the system is periodically forced, as in the dynamics of rotor blades in forward flight, the independent variable t (or the azimuth angle ψ) has to be converted to a state variable. Of course, one can always designate the time t or azimuth angle ψ as additional states, in order to transform the system to an autonomous one. This can either be achieved by $\dot{\psi} = \Omega$, where ψ is a state or by $\dot{t} = 1$, where t is a state and the azimuth angle can be calculated as $\psi = \Omega\, t$ since Ω can be assumed constant. However, if the above method is used (either cases), the new time state will monotonically increase and hence will not describe an oscillatory behaviour. Therefore, to solve this problem, a harmonic oscillator model can be used to realise the periodicity of all states. The harmonic oscillator equations are:

$$\begin{array}{rcrcrcl} \dot{u} &=& u &+& \Omega\, y &-& u\,(u^2+y^2) \\ \dot{y} &=& -\Omega\, u &+& y &-& y\,(u^2+y^2) \end{array} \tag{2}$$

or

$$\begin{array}{rcrcrcl} u' &=& u &+& y &-& u\,(u^2+y^2) \\ y' &=& u &+& y &-& y\,(u^2+y^2) \end{array} \tag{3}$$

where the $u = \sin(\Omega\, t)$ and $y = \cos(\Omega\, t)$ are solutions to Equation (2). The terms u and y can now be used to replace any $\sin(\Omega\, t)$, $\sin(\psi)$, $\cos(\Omega\, t)$ or $\cos(\psi)$ in the blade forcing equations as appropriate. Alternatively, the azimuth angle can be calculated using the quadrant-arctangent function (`atan2` function in MATLAB or FORTRAN).

$$\psi = \text{atan2}(u, y)$$

Rigid Blade Model with Flexible Hinges

In this section, continuation and bifurcation methods are applied to investigate the flap-lag stability of a rigid helicopter blade with springs attached between the blade root and rotor shaft, in the flap and lag degrees of freedom. This spring model is sufficient to represent an elastic blade and hub with hinge offsets. The model used here is published by Peters [7].

Equations of Motion

The equations of motion of the rotor blade in the flap and lag degrees of freedom are given by:

$$\begin{aligned} &\beta'' + \sin\beta\cos\beta(1+\zeta')^2 + (P-1)(\beta-\beta_{pc}) \\ &\quad + Z\zeta = \tfrac{1}{\Omega^2 I}\textstyle\int_0^R F_\beta r dr \\ &\cos^2\beta\zeta'' - 2\sin\beta\cos\beta(1+\zeta')\beta' + W\zeta \\ &\quad + Z(\beta-\beta_{pc}) = \tfrac{\cos(\beta)}{\Omega^2 I}\textstyle\int_0^R F_\zeta r dr \end{aligned} \tag{4}$$

where P, Z and W are stiffness parameters which depend on the non-rotating flap and lead-lag frequencies ω_β and ω_ζ. F_β and F_ζ are the force components per unit length perpendicular and parallel, respectively, to the direction of rotation. The expressions for the stiffness parameters and the force components are given in reference [7].

Rotor Model in the State Space Form

The main model equations, which have been generated in Equations (3) and (4) can be rearranged in terms of time derivatives of the state vector x to produce the required state-space form for the stability analysis:

$$x' = \begin{Bmatrix} u \\ y \\ \beta' \\ \beta'' \\ \zeta' \\ \zeta'' \end{Bmatrix} = f(x,\delta) \qquad \text{where} \qquad x = \begin{Bmatrix} u \\ y \\ \beta \\ \beta' \\ \zeta \\ \zeta' \end{Bmatrix} \quad (5)$$

where $\delta = \{\mu, \lambda, \theta_{col}, A_{lat}, B_{long}, \omega_\beta, \omega_\zeta, \ldots\}^T$.

Aeroelastic Rotor Blade Model

In this section, modal representation is used for the structural blade dynamics and hence each blade is represented by a number of general modes (eight in this analysis). The mode shapes, frequencies, and modal masses are computed a priori either in vacuum or at a given hover case condition. Although the model can include the dynamical equations for all blades of the rotor, it is adequate here to use a single bladed rotor model for the stability analysis.

The forced response equation approach is used to describe the aeroelastic dynamics of the blade. The equations used were developed in reference [21]. The formulation of this equation was done in a manner such that the orthogonality of the modes led to an equation in which the modal response depends only on the following forcing components:

1. the aerodynamic forcing;
2. time dependent terms such as the Coriolis force;
3. blade pitch dependent terms;
4. nonlinear terms not included in the formulation of the modal equation.

For the aerodynamic forcing, a blade element technique is used for calculating the forces and moments acting on the blades. This technique is based on dividing each blade into a number of elements, then the aerodynamic forces are computed for each element, considering them as quasi-two-dimensional aerofoils, with associated lift, drag and pitching moment characteristics. To achieve this, elemental velocity components need to be determined. Unsteady aerodynamics, blade/blade and blade/airframe interactions are not considered here. To model the inflow, a three state dynamic induced velocity model is used. The code of this model is written in MATLAB.

Modal Response Equation

The forced response equation for each mode is:

$$\ddot{q}_i + \omega_{q_i}^2 \, q_i = \frac{Q_{q_i}}{I_i} \qquad i = 1,2,3,\ldots \quad (6)$$

hence

$$\ddot{q}_i = -\omega_{q_i}^2 \, q_i \; + \; \frac{Q_{q_i}}{I_i} \qquad i = 1,2,3,\ldots \quad (7)$$

where ω_{q_i}, I_i, q_i and Q_{q_i} are the modal frequency, modal mass, generalised displacement and generalised force terms for each mode i. The differentiation $(\ddot{})$ is done with respect to time t. It can be noticed from equation (6) that the elastic damping is assumed negligible and hence is not accounted for. Each mode shape consists of flap, lag and twist mode shape components, w_i, v_i and t_i respectively. The generalised force Q_{q_i} consists of the four forcing terms described above and can be written as follows:

$$Q_{q_i} = Q_{aero,q_i} + Q_{tdep,q_i} + Q_{pper,q_i} + Q_{nlin,q_i} \quad (8)$$

where the expressions for the forcing terms can be found in [21].

Local Flow Velocities

The blade deformation due to bending and twisting affects the local flow velocities and also angles of attack. In general, the components of the resultant flow velocity at each blade element arise from five sources, namely: blade rotation, free stream due to the helicopter movement, rotor induced velocity, rates of blade bending and rates of change of the predeformed blade coordinates. Furthermore, the resultant flow velocity is conventionally resolved into components tangential (U_T) and normal (U_P) to the local axes of the blade. The full expressions of these components depend on many variables, including the positions of the blade elements before and after deformation, and can be very long. Hence, they are not presented here but can be found in [21].

Blade Aerodynamics

The aerodynamic forcing Q_{aero,q_i} in Equation (8) is the most complex term to evaluate in comparison to the rest

of the forcing terms. This is due to the complicated nature of the flow field around the aerofoil section. The general form of Q_{aero,q_i} is given by the integral:

$$Q_{aero,q_i} = \int_0^R \left[\frac{d(L-L_0)}{dr} w_i + \frac{d(D+D_0)}{dr} v_i + \frac{d(M-M_0)}{dr} t_i \right] dr \quad (9)$$

where the three terms on the right hand side represent the force distribution in the flapwise and lagwise direction and the pitching moment distribution respectively.

To evaluate the above aerodynamic loads, the elemental lift and drag forces and pitching moment need first to be calculated. In this analysis, the blade element method is adopted an hence two-dimensional quasi-steady flow is assumed. The expression for the elemental lift, drag and pitching moment are given as:

$$\delta L = \frac{1}{2}\rho U^2 c \delta r C_L(\alpha, Ma, r) \quad (10)$$

$$\delta D = \frac{1}{2}\rho U^2 c \delta r C_D(\alpha, Ma, r) \quad (11)$$

$$\delta M = \frac{1}{2}\rho U^2 c^2 \delta r C_M(\alpha, Ma, r) \quad (12)$$

where ρ, c, $U = \sqrt{U_P^2 + U_T^2}$, δr, C_L, C_D and C_M are the local air density, the blade elemental chord, the elemental resultant flow velocity, the width of the blade element, and the lift, drag and pitching moment coefficients at each element respectively. α and Ma are the elemental angle of attack and Mach number respectively. The aerodynamic force and moment coefficients for each individual blade element are calculated numerically using nonlinear look-up tables. Experimental data for chosen aerofoil sections are used. These tables provide data for a 360° range of angle of attack and local Mach numbers of up to 0.85. The local angle of attack is given by:

$$\alpha = \theta + \phi + \theta_{quasi} \quad (13)$$

where θ is the elemental pitch angle, $\theta_{quasi} = \frac{c\dot{\theta}}{2U}$ is the aerodynamic quasi-steady effect on pitch angle and ϕ is the elemental inflow angle, which can be calculated as follows:

$$\phi = \text{atan2}(U_P, U_T)$$

The local pitch angle θ is a combination of all the local pitch angle contributions, i.e.:

$$\theta = \theta_{col} - A_{lat}\cos(\psi) - B_{long}\sin(\psi) + \theta_{pre.twist} + \Theta$$

where θ_{col}, A_{lat},B_{long}, $\theta_{pre.twist}$ and Θ are the blade collective pitch, the lateral cyclic, the longitudinal cyclic, the blade local built-in twist and the blade pitch due to twist deformation.

Finally, the local forces acting on a blade element in the blade coordinate system can therefore be determined from the elemental lift and drag forces.

$$\begin{aligned} L &= \delta L \sin\phi - \delta D \cos\phi \\ D &= -\delta L \cos\phi - \delta D \sin\phi \end{aligned} \quad (14)$$

whereas, the local elemental aerodynamic pitching moment is simply defined as:

$$M = \delta M \quad (15)$$

The rotor instantaneous thrust T_i can be evaluated simply by summing all elemental vertical forces L and multiplying it by the number of blades NB. i.e.

$$T_i = NB \sum_{elem=1}^{N} L \quad (16)$$

This value of thrust is only used to estimate the induced velocity within the rotor model. The correct thrust value, which is used for performance and trimming procedures, has to be averaged out across one rotor revolution.

$$T_{av} = \frac{1}{2\pi}\int_0^{2\pi} T_i \, d\psi \quad (17)$$

Induced Velocity Model

The inflow is captured via a 3-state Pitt-Peters dynamic wake model [22, 23, 24]. This model permits the variations of the induced velocity in both the radial and azimuthal position. Furthermore, it allows the lag dynamics associated with moving a volume of air to be modelled. The inflow model is given for three states as follows:

$$\nu_i(r,\psi) = \nu_0 + \frac{r}{R}(\nu_s sin\psi + \nu_c \cos\psi) \quad (18)$$

where ν_i is the induced velocity at an element of radius r and azimuth position ψ. The induced velocity components ν_0, ν_s and ν_c are given in the wind axes by:

$$[\tau]\begin{bmatrix} \dot{\nu_0} \\ \dot{\nu_s} \\ \dot{\nu_c} \end{bmatrix}_w = -\begin{bmatrix} \nu_0 \\ \nu_s \\ \nu_c \end{bmatrix}_w + [L]\begin{bmatrix} T_{aero} \\ L_{aero} \\ M_{aero} \end{bmatrix}_w \quad (19)$$

T_{aero}, L_{aero} and M_{aero} are the thrust, the aerodynamic rolling and pitching moments respectively in the wind axis and expressions for the matrices $[\tau]$ and $[L]$ can be found in [22, 23, 24].

Rotor Model in the State Space Form

The main model equations, which have been generated in Equations (2), (7) and (19), can be rearranged in terms

of time derivatives of the state vector x to produce the required state space form:

$$\dot{x} = \begin{Bmatrix} \dot{u} \\ \dot{y} \\ \dot{\nu}_0 \\ \dot{\nu}_s \\ \dot{\nu}_c \\ \dot{q}_1 \\ \ddot{q}_1 \\ \vdots \\ \dot{q}_8 \\ \ddot{q}_8 \end{Bmatrix} = f(x,\delta) \quad \text{where} \quad x = \begin{Bmatrix} u \\ y \\ \nu_0 \\ \nu_s \\ \nu_c \\ q_1 \\ \dot{q}_1 \\ \vdots \\ q_8 \\ \dot{q}_8 \end{Bmatrix} \quad (20)$$

CONTINUATION AND BIFURCATION RESULTS

Rigid Blade Model with Flexible Hinges

In order to find the steady state or periodic solutions for the rigid blade model as given in Equation (5), the inflow ratio λ and the control angles θ_{col}, A_{lat} and B_{long} need to be known for a given set of μ, ω_β, etc. Of course, the analysis can be carried out at a prescribed values of λ, θ_{col}, A_{lat} and B_{long}. However, the conventional way is to compute λ based on a momentum theory assumption, and find the control angles which satisfy the intended trim requirements.

Unlike many analyses, where rotor trimming is carried out first (using the harmonic balance method for example) prior to any stability calculations, AUTO can compute solutions and their stability simultaneously for given boundary or integral conditions. This means that the continuation and trimming procedure can be done in parallel. In fact, the eigenvalues and Floquet multipliers are computed at negligible extra cost to the continuation analysis. To find λ, θ_{col}, A_{lat} and B_{long} four integral boundary conditions are constructed as follows:

1. λ is obtained by equating the thrust calculated by integrating the vertical force along the blade to the thrust from simple momentum theory:

$$2\nu\sqrt{\mu^2+\lambda^2} - \frac{\sigma a}{2\pi\gamma}\cos\beta\int_0^{2\pi}\frac{1}{\Omega^2 I}\int_0^R F_\beta r dr d\psi = 0 \quad (21)$$

where the induced velocity ν is given by:

$$\nu = \lambda - \mu\alpha_s$$

and α_s is the rotor shaft angle, which can be obtained from the propulsive time condition

$$\alpha_s = \frac{\mu^2 \bar{f}}{2C_T}$$

where $\bar{f}$ is the helicopter flat plate drag area. $\bar{f}$ can be set to zero if propulsive trim is not required.

2. θ_{col} is obtained by equating the calculated thrust obtained by integrating the vertical force along the blade to the required thrust:

$$C_{T,req} - \frac{\sigma a}{2\pi\gamma}\cos\beta\int_0^{2\pi}\frac{1}{\Omega^2 I}\int_0^R F_\beta r dr d\psi = 0 \quad (22)$$

3 & 4 To find A_{lat} and B_{long}, moment trim condition is assumed at the rotor hub. This condition is obtained by suppressing the first harmonic components of the flapping angle using the cyclic pitch angles. This is implemented as follows:

$$\int_0^{2\pi}\beta\,\sin\psi\,d\psi = \int_0^{2\pi}\beta\,u\,d\psi = 0 \quad (23)$$

$$\int_0^{2\pi}\beta\,\cos\psi\,d\psi = \int_0^{2\pi}\beta\,y\,d\psi = 0 \quad (24)$$

It should be noted that high harmonic components of the blade flapping angle are not suppressed by Equations (23) and (24).

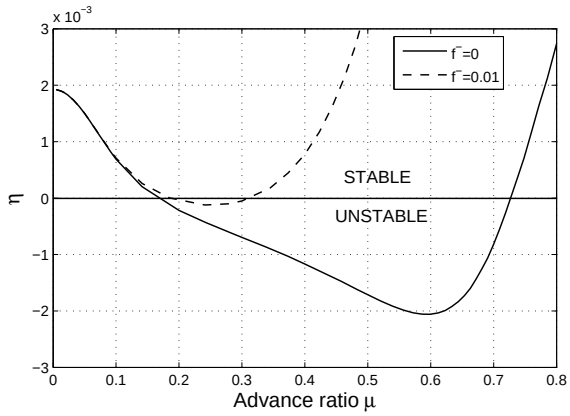

Figure 1: Lag damping variation with advance ratio. $p = 1.15$, $\omega_\zeta = 1.4$, $\bar{R} = 0$, $\gamma = 5$, $\sigma = 0.05$, $C_{d_0} = 0.01$, $C_T/\sigma = 0.2$.

The rigid blade model was coded in MATLAB, and AUTO was supplied with the state-space equations of the model and the four integral conditions, i.e. equations (5), (21), (22), (23) and (24). The continuation was performed at two cases of trim condition. The first is a propulsive trim at $\bar{f} = 0.01$ and the second is a moment trimmed condition in which $\bar{f} = 0$. In order to compare the continuation results with those published by Peters [7], the damping parameter η associated with the lag degree of freedom is extracted from the computed Floquet multipliers ϑ. To find η the logarithm of the Floquet multiplier associated with the lag mode is evaluated to find the equivalent eigenvalue. Then η is simply the negative real part of this eigenvalue ($\eta = -\Re(\ln\vartheta)$).

Figure 1 shows the variation of lag damping with advance ratio for $\bar{f} = 0$ and $\bar{f} = 0.01$. Like the predictions of Peters, the results illustrate that the lag mode becomes

unstable at certain ranges of advance ratios. The damping graph for the case $\bar{f} = 0.01$ is identical to the graph predicted by Peters. However, for the case $\bar{f} = 0$, although η becomes negative at the same μ predicted by Peters (≈ 0.16), the value at which η becomes positive again is higher when using the continuation method (≈ 0.73 compared to ≈ 0.49). This discrepancy is thought to be due to the different trimming procedures. Peters used the harmonic balance method where second and higher harmonics of the blade flapping were assumed negligible, whereas no such assumptions were used in the continuation analysis. In fact, although the first flap harmonics were suppressed to ensure moment trim requirement, it can be shown that the second flap harmonics are large for $\mu > 0.4$, when the trimming is achieved using the continuation approach. Therefore, the values of the control angles evaluated by the two approaches can be different.

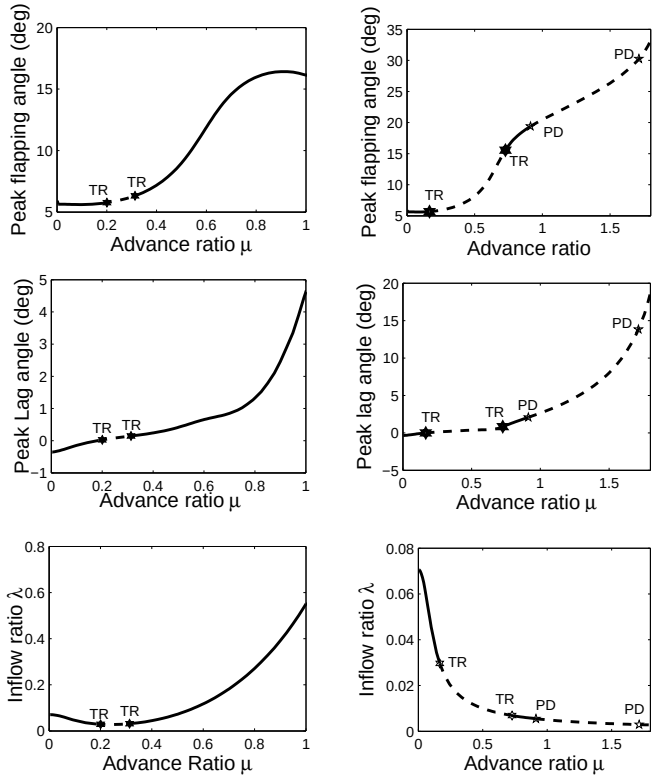

(a) $\bar{f} = 0.01$ (b) $\bar{f} = 0$

Figure 2: Bifurcation diagrams for the cases $\bar{f} = 0.01$ and $\bar{f} = 0$. Continuation parameter = μ. Solid line: stable periodic branch, dashed line: unstable periodic branch. For the flap and lag angles, only the peak values of the oscillations in one cycle are plotted. TR denotes torus bifurcations.

Figure 2 depicts the bifurcation diagrams for the cases of $\bar{f} = 0.01$ and $\bar{f} = 0$ respectively. The variation of inflow ratio λ computed by AUTO is also plotted for completeness. The bifurcation diagrams show that the change in stability of the periodic branches, as previously predicted by η changing sign in Figure 1, corresponds to the presence of *torus (Neimark-Sacker)* bifurcation points. This type of bifurcation occurs when a pair of complex conjugates of the Floquet multipliers cross the unit circle (in the real and imaginary plane) at a non zero real part. Furthermore, a new secondary quasi-periodic branch (branch of invariant tori) emerge from the bifurcation points. To investigate this further, the rotor model was simulated in time from the unstable branch at $\mu = 0.5$ for the case of $\bar{f} = 0$. The appropriate values for λ, θ_{col}, A_{lat} and B_{long} were used. Figure 3 illustrates that the flapping angle oscillation starts from the unstable periodic solution (limit cycle) and then diverges to a stable quasi-periodic solution. The unstable periodic solution has a time period of 1 rev (2π rad), while it is not possible to identify an oscillation period for the stable quasi-periodic behaviour of the blade flapping motion. To further verify that the solution is quasi-periodic, a segment of the time response was plotted in both $(\psi, \beta, \dot{\beta})$ and $(\psi, \zeta, \dot{\zeta})$ cylindrical coordinate systems. It can be shown that solution trajectories trace the surface of a torus but do not connect.

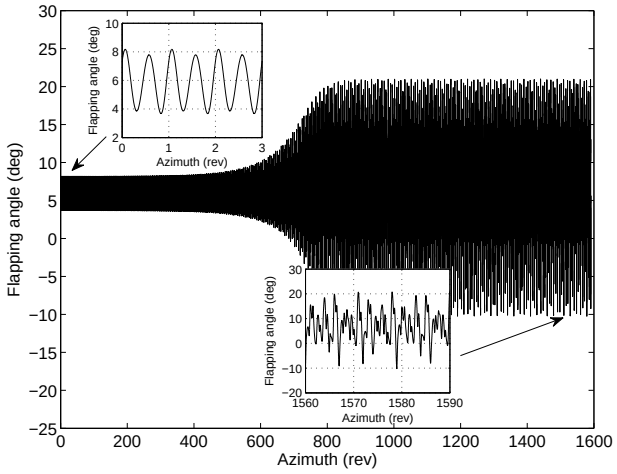

Figure 3: Time simulation from unstable branch at $\mu = 0.5$ and $\bar{f} = 0$. $p = 1.15$, $\omega_\zeta = 1.4$, $\bar{R} = 0$, $\gamma = 5$, $\sigma = 0.05$, $C_{d_0} = 0.01$, $C_T/\sigma = 0.2$.

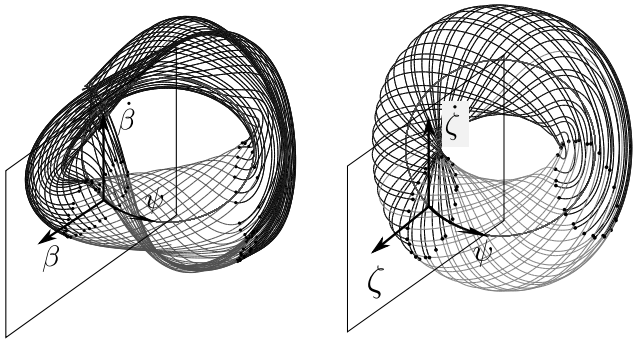

(a) Flap DOF (b) Lag DOF

Figure 4: Segment of the stable quasi-periodic solution traces a surface of a torus in a cylindrical coordinate frame of axes. $\mu = 0.5$, $\bar{f} = 0$, $p = 1.15$, $\omega_\zeta = 1.4$, $\bar{R} = 0$, $\gamma = 5$, $\sigma = 0.05$, $C_{d_0} = 0.01$, $C_T/\sigma = 0.2$.

Two more characteristics of the unstable periodic branch can be observed from Figure 3. First, it can be seen that the second harmonics are evident in the flapping motion and are not suppressed. Second, the time taken for the flapping motion to clearly diverge from the

unstable periodic orbit toward the quasi-periodic solution is very high (about 400 revolutions), which may lead the solutions to appear to be stable. This means that a good level of accuracy in the stability method is necessary to predict the correct stability for this system at this parameter combination. Figure 2-(b) also illustrates the presence of *period doubling* bifurcations at high advance ratios. The first bifurcation occurs at $\mu \approx 0.9$ where the main stable periodic branch becomes unstable, whereas the second bifurcation is at an even higher value of μ. Period doubling bifurcation occurs when one Floquet multiplier equals -1 with zero imaginary part. After the bifurcation point, the main periodic branch changes stability and a new secondary periodic branch emerges. The periodic solutions of this secondary branch have double the period of the solutions of the main branch. To illustrate this point, the rotor model was simulated in time from the unstable branch at $\mu = 1$ for the case of $\bar{f} = 0$. The appropriate values for λ, θ_{col}, A_{lat} and B_{long} were used. Figure 5 illustrates that the flapping angle oscillation starts from the unstable periodic solution (limit cycle) and then diverges to another stable periodic solution. The unstable main periodic solution has a time period of 1 rev, while the other secondary periodic solution has a time period of 2 rev (3 cycles between 1584 and 1590 rev).

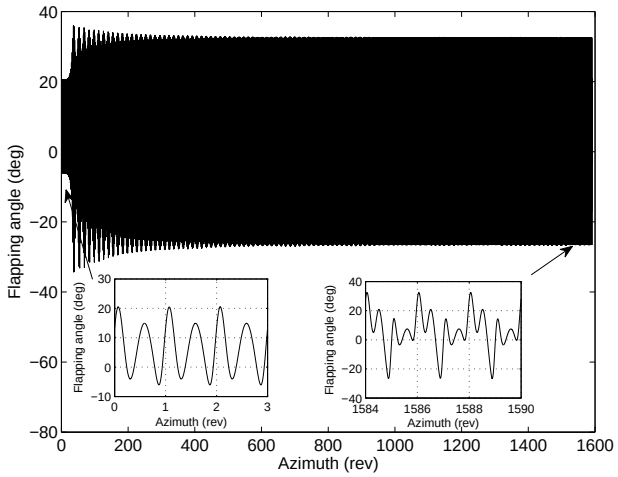

Figure 5: Time simulation from unstable branch at $\mu = 1.0$ and $\bar{f} = 0$. $p = 1.15$, $\omega_\zeta = 1.4$, $\bar{R} = 0$, $\gamma = 5$, $\sigma = 0.05$, $C_{d_0} = 0.01$, $C_T/\sigma = 0.2$.

Aeroelastic Rotor Blade Model

Similar to the rigid blade analysis, the rotor trim conditions were also embedded within the continuation procedure. Since a dynamic inflow model is used in this case, only three integral conditions were needed to be specified. These can be described as follows:

$$T_{av} = \frac{1}{2\pi}\int_0^{2\pi} T_i \, d\psi = T_{req} \tag{25}$$

$$\frac{1}{\pi}\int_0^{2\pi} \beta \, \sin(\psi) \, d\psi = \frac{1}{\pi}\int_0^{2\pi} \beta \, u \, d\psi = \beta_{a_1,req} \tag{26}$$

$$\frac{1}{\pi}\int_0^{2\pi} \beta \, \cos(\psi) \, d\psi = \frac{1}{\pi}\int_0^{2\pi} \beta \, y \, d\psi = \beta_{b_1,req} \tag{27}$$

The rotor model was configured to have realistic blade and flight characteristics. Figure 6 illustrates the continuation results when the advance ratio was used as the continuation parameter. Only the peak values of oscillatory modal displacements of the first two modes are plotted. The bifurcation diagrams show that when μ is between approximately 1.03 and 1.19 the periodic branch is unstable, due to the presence of two torus bifurcations. To further scrutinise the results, the variation of the damping of the modes was investigated from the computed Floquet multipliers. It was found that the unstable periodic branch corresponds to the range of advance ratios when the damping of the first lag mode (mode 1) is negative. Hence, this indicates that this instability may be of the flap-lag type similar to the one obtained in the previous section.

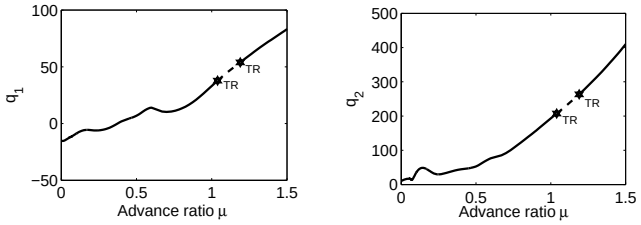

Figure 6: Bifurcation Diagram for forward flight case. Continuation parameter = μ. Solid line: stable periodic branch, dashed line: unstable periodic branch. Only the peak values of the oscillations in one cycle are plotted. TR denotes torus bifurcations.

It should noted that although the model might not be suited for flight conditions of very high advance ratios ($\mu > 0.5$ for example), it is customary when performing continuation analysis to extend the continuation parameter beyond the physical range. The reason for this is to search for any bifurcation points that might lead to new solution branches, which return back to the physical range. For the case investigated in Figure 6, the only secondary branch found was the quasi-periodic branch, for $1.03 \leq \mu \leq 1.19$ emerging from the torus bifurcations points.

Continuation runs were also carried out in the hover case over a range of collective pitch angles. The resulting bifurcation diagrams are depicted in Figure 7. In stable hover condition, the blade is in steady state situation and hence its behaviour is not periodic. For this reason there is no need to use neither the harmonic oscillator method, since there is no periodic forcing to the system, nor to trim the rotor to certain flapping angle components. Furthermore, since the collective pitch is used as the continuation parameter, which will directly affect rotor thrust, the integral thrust condition is not necessary for this case.

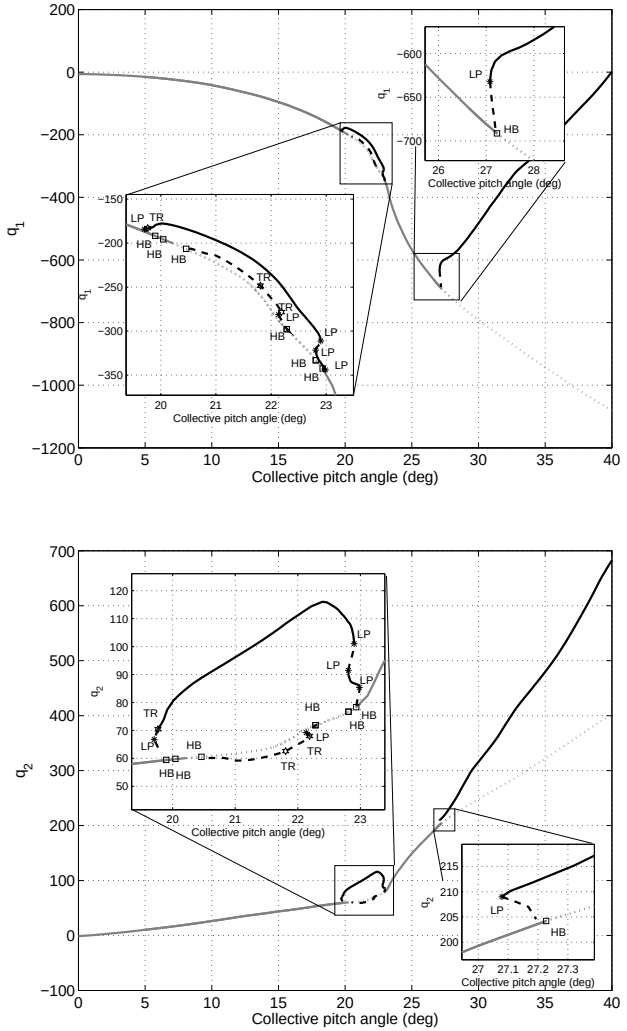

Figure 7: Bifurcation Diagram for hover case. Continuation parameter = θ_{col}. Black solid line: stable periodic branch, black dashed line: unstable periodic branch, gray solid line: stable equilibrium branch, dotted gray line: unstable equilibrium branch. Only the peak values of the periodic oscillations in one cycle are plotted. TR, HP and LP denotes torus, Hopf and limit point (fold) bifurcations respectively.

As θ_{col} is increased from 0°, there is only one stable equilibrium (hover) branch, which becomes unstable between 19.8° and 23°. This equilibrium branch also distabilises at θ_{col} higher than 23°. In the first instability case, the main branch changes stability at two Hopf bifurcation points located at 19.8° and 23°. This type of bifurcation occurs when a complex conjugate pair of eigenvalues cross the imaginary axis, of the real and imaginary plane, with non zero imaginary parts. Hopf bifurcation is also associated with the birth of secondary periodic solutions. In Figure 7, both Hopf points are subcritical leading to the birth of unstable periodic solutions, which co-exist with sections of the stable equilibrium branch. Subcritical Hopf is a hard bifurcation which will lead to the solutions to jump to another attractor just after the bifurcation point. This jump can be very hazardous. The unstable periodic branch emerging from the Hopf point at $\theta_{col} = 19.8^\circ$ extends very slightly as θ_{col} is reduced and then it folds back at a limit point (fold bifurcation) at $\theta_{col} = 19.6^\circ$. This bifurcation point occurs when one Floquet multiplier crosses the unit circle at a value of 1. The solution then becomes stables and extends as θ_{col} is increased. Furthermore, this stable periodic branch changes stability a few times in the vicinity of $\theta_{col} = 23^\circ$ due to the existence of three other fold bifurcation points, until it merges with the main equilibrium branch at the Hopf point located at $\theta_{col} = 23^\circ$. It can be shown that if the blade is disturbed from the unstable equilibrium branch, it will always get attracted to the stable periodic branch. In other words, if the pitch angle is between 19.8° and 23°, the blade will eventually behave in a periodic manner.

The Hopf point at $\theta_{col} = 19.8^\circ$ is found to be associated with the first flap mode becoming unstable, which stabilises again at $\theta_{col} = 23^\circ$. It was also found that other two flap modes lose and gain stability within the same range of pitch angles. This is depicted by other four Hopf bifurcation points within the unstable equilibrium branch. The unstable periodic branch which emerge from two of these points is plotted in Figure 7. This branch also experience torus bifurcations.

Figure 7 also illustrates the existence of a subcritical Hopf and limit point bifurcation, which fold the secondary unstable periodic branch into a stable periodic one. If the pich angle is increased beyond 27.23°, the solutions will jump to the stable periodic branch. It can be also seen that in the range $\theta_{col} = 27.07^\circ$ to 27.23° the blade can behave either in a stable equilibrium or in a stable periodic manner, depending on the perturbation levels subjected to the blade. Although this pitch range is small and non-operational, it provides a good example on how important the construction of the bifurcation diagram is in predicting the global nonlinear dynamics of the blade behaviour.

CONCLUSION

This paper presented an implementation of continuation and bifurcation methods in studying the aeroelastic stability of helicopter blades over a range of advance ratios and blade pitch angles. The set up for the continuation analysis and the general blade modelling layout were described for two different nonlinear blade models. These aeroelastic models were constructed in a generic state space form, where the harmonic oscillator approach was used to transform the periodically forced equations into autonomous ones. Furthermore, the paper described how the trimming procedure is implemented within the continuation analysis, in which the appropriate integral conditions describing the trim requirements were presented.

The continuation analysis was first applied to a simple rotor system incorporating rigid blade with flap and lag degrees of freedom with root springs to model the

stiffness of hinges. The continuation results were compared to published blade flap-lag stability data and explained in the light of bifurcation theory. One of the key advantages of the method was the ability to identify the types of bifurcations which led to blade instabilities. This in turn helped in predicting the new secondary periodic branches, leading to a better understanding of the global blade dynamics. The bifurcations discussed for this model were torus and period doubling bifurcations.

The continuation and bifurcation analysis was also applied to investigate the aeroelastic stability of a flexible rotor blade, where in this case modal representation of the blade flexibility is used. This representation is widely adopted in the helicopter industry. The continuation results were also explained in the light of bifurcation theory for both forward flight and hover conditions. The results illustrated that even in the hover case the global nonlinear dynamics of the blade are quite complex. The bifurcations discussed in this case were Hopf, fold and torus bifurcations.

The analysis presented in this paper not only illustrated that continuation and bifurcation methods are applicable to studying the blade aeroelastic stability, but also confirmed that the dynamics of the blade behaviour are very complex and nonlinear, even in the hover condition. Although most of the complex behaviour of the blade was found at a non-operational parameter range, the continuation and bifurcation tools were essential in uncovering the global blade dynamics when multiple solutions coexist. Therefore, these tools offer considerable advantages in aeroelastic stability analyses of future rotor configurations, in particular, when the nonlinearity is significant. They are likely to offer valuable efficiencies for analyses of, for example, blades incorporating active trailing edge flaps or semi-active lag dampers.

ACKNOWLEDGMENT

The authors would like to thank AgustaWestland for funding and supporting of the work presented in this paper.

References

[1] A. Gessow and A. D. Crim. A method of studying the transient blade-flapping behaviour of lifting rotors at extreme operating conditions. NACA.3366, January 1955.

[2] G. Horvay. Rotor blade flapping motion. *Quart. Appl. Math*, Vol. 5, No. 2, 1947, pp. 149-167.

[3] G. Horvay and S. W. Yuan. Stability of rotor blade flapping motion when the hinges are tilted: Generalization of the 'rectangular ripple' method of solution. *Journal of the Aeronautical Sciences*, 1947, pp. 583-593.

[4] A. G. Shutler and J. P. Jones. The stability of rotor blade flapping motion. Aeronautical Research Council, R & M No. 3178, May 1958.

[5] O. J. Lowis. The stability of rotor blade flapping motion at high tip speed ratios. Aeronautical Research Council, R & M No. 3544, January 1963.

[6] F-S. Wei and D.A. Peters. Lag damping in autorotation by a pertubation method. *Proceedings of the American Helicopter Society 34th Annual Forum*, pages 78–25, May 15-17, 1978.

[7] D. A. Peters. Flap-lag stability of helicopter rotor blades in forward flight. *Journal of American Helicopter Society*, Vol. 20, No. 4, October 1975.

[8] D. A. Peters and K. Hohenemser. Application of the floquet transition matrix to problems of lifting rotor stability. *Journal of American Helicopter Society*, Vol. 16, No. 2, October 1971.

[9] D.A. Peters and K.H. Hohenemser. Application of the Floquet transition matrix to problems of lifting rotor stability. *Journal of the American Helicopter Society*, 26:25–33, 1970.

[10] P. P. Friedmann and D. H. Hodges. Rotary wing aeroelasticity - a historical perspective. *Journal of Aircraft*, Vol. 40, No. 6:1019–1046, November-December 2003.

[11] P. P. Friedmann and D. H. Hodges. Rotary-wing aeroelasticity: Current status and future trends. *AIAA Aircraft*, Vol. 42, No. 10:1953–1972, October 2004.

[12] R. L. Bielawa. *Rotary Wing Structural Dynamics and Aeroelasticity*. AIAA (American Institute of Aeronautics & Ast, 2006.

[13] I. Chopra. Perspectives in aeromechanical stability of helicopter rotors. *Vertica*, Vol. 14, No. 4, 1990, pp. 457-508.

[14] D. Rezgui, P. C. Bunniss, and M. H. Lowenberg. The stability of rotor blade flapping motion in autorotation using bifurcation and continuation analysis. *Proceedings of 32nd European Rotorcraft Forum*, 2006.

[15] D. Rezgui, M. H. Lowenberg, and P. C. Bunniss. Experimental and numerical analysis of the stability of an autogyro teetering rotor. *Proceedings of the American Helicopter Society 64th Annual Forum*, April 2008.

[16] D. Rezgui, M. H. Lowenberg, and P. C. Bunniss. A combined numerical/experimental continuation approach applied to nonlinear rotor dynamics. *Proceedings of the European Consortium for Mathematics in Industry (ECMI)*, 2008.

[17] M. H. Lowenberg, D. Rezgui, and P. C. Bunniss. Experimental evaluation of numerical continuation and bifurcation methods applied to autogyro rotor blade aeromechanical stability. *Proceedings of the ASME 2009 International Design Engineering Technical Conferences & Computers and Information in Engineering Conference*, August-September 2009.

[18] Y.A. Kuznetsov. *Elements of Applied Bifurcation Theory*. Springer-Verlag, 1995.

[19] J. Guckenheimer and P. Holmes. *Nonlinear Oscillations, Dynamical Systems and Bifurcations of Vector Fields*. Springer, 1993.

[20] E. J. Doedel, B. E. Oldeman, A. R. Champneys, F. Dercole, T. F. Fairgrieve, Yuri A. Kuznetsov, R. C. Paffenroth, B. Sandstede, X. J. Wang, and C. Zhang. AUTO-07P : Continuation and bifurcation software for ordinary differential equations. Technical report, Concordia University, Montreal, Canada, 2009. http://indy.cs.concordia.ca/auto/.

[21] Rotor Systems Group Report. Users specification for R150. Technical Report RSG/00/0217, Issue 2, AgustaWestland, May 2002.

[22] D.M. Pitt and D.A. Peters. Theoretical prediction of dynamic inflow derivatives. *Vertica*, Vol. 5, 1981, pp. 21-34.

[23] D. A. Peters and N. HaQuang. Dynamic inflow for practical applications. *Journal of American Helicopter Society*, Vol. 33, No. 4, 1988, pp. 64-68.

[24] G.H. Gaonkar and D.A. Peters. Review of dynamic inflow modelling for rotorcraft flight dynamics. *Vertica*, Vol. 12, No. 3, 1988, pp. 213-242.